https://doi.org/10.5194/egusphere-2025-5433
Preprint. Discussion started: 18 November 2025

Seasonal dynamics of closed lakes nutrient status controlled by lacustrine groundwater discharge

Xiaoliang Sun[1,2], Yao Du[1,2*], Hao Tian[1,2], Jiawen Xu[1,2], Huanhuan Shi[1,2], Yetong Liu[1,2], Yamin Deng[1,2], Yiqun Gan[1,2], Yanxin Wang[1,2]

[1]Key Laboratory of Groundwater Quality and Health (China University of Geosciences), Ministry of Education, Wuhan 430078, China.

[2]School of Environmental Studies & State Key Laboratory of Geomicrobiology and Environmental Changes, China University of Geosciences, Wuhan 430078, China.

Corresponding: Yao Du (yaodu@cug.edu.cn)

Abstract. Lacustrine groundwater discharge (LGD) and its associated nitrogen (N) and phosphorus (P) inputs are increasingly recognized as the critical drivers of lake eutrophication. However, the intermonthly variability in LGD and its influence on lake nutrient dynamics remain poorly understood. In this study, high-frequency monitoring and hydrochemical analyses were conducted over a full hydrological year to investigate LGD-related nutrient fluxes and their effects in a typical oxbow lake in the central Yangtze Basin. Water level data and ^{222}Rn tracing revealed a seasonal LGD pattern characterized by an increase followed by a decline, ranging from 35.36 to 51.71 $mm \cdot d^{-1}$. This pattern was regulated by monthly net precipitation, which controlled the lake level fluctuations and LGD rates. The corresponding N and P loads varied synchronously with LGD and showed seasonal synchrony with lake N and P concentrations. Moreover, variations in the N/P ratio carried by LGD regulate the lake water N/P ratio, thereby influencing its relationship with the dynamic changes in chlorophyll-a. From a global perspective, in closed lakes, LGD is typically governed by climatic factors such as precipitation and evaporation, thereby serving as a key process regulating the lake's trophic status. This study provides the first evidence that groundwater-driven nutrient loading influences lake nutrient status on an intermonthly scale offering new insights and management strategies for eutrophication control in shallow, closed lake systems worldwide.

1 Introduction

Lakes are vital terrestrial ecosystems with ecological, environmental, and societal importance

https://doi.org/10.5194/egusphere-2025-5433
Preprint. Discussion started: 18 November 2025

(Zedler and Kercher, 2005). A number of studies have highlighted that lacustrine groundwater discharge (LGD) not only sustains the lake water balance but also serves as a key pathway for nitrogen (N) and phosphorus (P) inputs, significantly influencing biogeochemical cycling (Meinikmann et al., 2015; Rosenberry et al., 2015; Luo et al., 2018; Kazmierczak et al., 2020; Lewandowski et al., 2024). By altering nutrient concentrations, LGD can regulate lake trophic status and contribute to eutrophication (Shi et al., 2022; Zheng et al., 2024). Thus, understanding LGD's impact on lake water environments is critical for elucidating eutrophication mechanisms.

The LGD rate shows pronounced temporal variability over the hydrological year, primarily driven by meteorological and hydrological factors (Burnett et al., 2017; Shi et al., 2022; Sun et al., 2024). For relatively closed lake systems, meteorological factors are typically the primary drivers of LGD variation. Although precipitation, evaporation, and temperature are known to influence LGD, their effects vary regionally. Positive correlations with evaporation have been observed in Taihu Lake (Shi et al., 2022), whereas negative correlations with both precipitation and evaporation have been observed in coal mining subsidence lakes (Jiang et al., 2024). In Permafrost regions, LGD is restricted to summer thaw periods (Walvoord & Striegl, 2007; Olid et al., 2022). However, the understanding of monthly scale LGD modulation by meteorological forcing remains limited, primarily because of the low observational frequency. In particular, the mechanistic linkages along the precipitation/evaporation → lake/groundwater level → LGD pathway require systematic investigation.

In some lakes, LGD contributes more than 50%, and in certain cases, over 90% of the total nitrogen (N) and phosphorus (P) inputs often exceed those from surface inflows (Stets et al., 2010; Meinikmann et al., 2015; Shi et al., 2022). Once discharged, groundwater-derived nutrients undergo biogeochemical transformations or are assimilated by aquatic organisms, thereby affecting the primary productivity and eutrophication (Zheng et al., 2025). For instance, LGD-driven nutrient inputs have been shown to stimulate chlorophyll a (Chl *a*) production in closed lakes and alter nutrient limitation patterns via shifts in N/P ratios (Xu et al., 2025). In Taihu Lake, LGD-derived N inputs were found to alleviate N limitation (Zheng et al., 2025). However, most studies have focused on nutrient flux quantification over discrete periods, with limited insight into the temporal variability and trophic responses of lakes.

The middle Yangtze River (YR) Plain features a dense lake network and strong groundwater-surface water interactions (Jiang et al., 2022; Hu et al., 2023). Regional groundwater often

https://doi.org/10.5194/egusphere-2025-5433
Preprint. Discussion started: 18 November 2025

contains N and P concentrations that are an order of magnitude higher than those in the surface waters (Du et al., 2020; Tao et al., 2020). LGD has been confirmed in various lake types, contributing to both water volume and solute budgets (Gan et al., 2023; Tian et al., 2025). However, its specific role in nutrient loading and eutrophication remains poorly understood. Heiwawu Oxbow Lake (HWL), situated along a former YR channel, provides a valuable setting to examine the temporal dynamics of LGD due to its seasonal hydrological connectivity. Typically isolated from the Yangtze by November, HWL experienced an earlier disconnection in August 2022 due to extreme drought (Sun et al., 2024). During this period, the lake's water and nutrient balance depended almost entirely on precipitation and groundwater, offering an ideal natural experiment to investigate LGD-driven nutrient loading and eutrophication over a complete hydrological year.

In this study, we quantified LGD and its associated nitrogen and phosphorus fluxes by conducting bi-monthly, high-frequency monitoring of groundwater and lake water levels, and by applying a ^{222}Rn mass balance model to a typical closed lake in the middle reaches of the Yangtze River. Furthermore, we examined the influence of meteorological factors on LGD and the dynamic effects of LGD-driven nutrient inputs on lake trophic status. The results elucidate the role of precipitation and evaporation in regulating the seasonal dynamics of LGD and highlight the critical influence of LGD on the nutrient regime of closed lakes. These findings provide a valuable scientific basis for improving water quality management and mitigating eutrophication in closed-lake systems worldwide.

2 Materials and Methods

2.1 Study area

HWL is situated in the southern Jianghan Plain on the northern bank of the middle reaches of the YR, between 29° 45' 10.98'' – 29° 48' 52.10'' N and 112° 41' 35.90'' – 112° 46' 32.16'' E (Figure 1a and b). The region has a subtropical monsoon climate, with an annual mean temperature of 15–17°C, average annual precipitation of approximately 1400 mm, and average annual evaporation of approximately 1100 mm. The area surrounding HWL is characterized by flat terrain with a slope of less than 0.1‰, and the dominant land use types include forest and farmland.

HWL was formed in 1967 following the artificial cutoff of a meander of the YR, with a downstream channel providing hydrological connectivity between the lake and the river. During the wet season, elevated YR water levels induce the inflow into HWL, whereas in the dry season, declining YR levels result in backflow from the lake into the river, ultimately leading to complete disconnection.

https://doi.org/10.5194/egusphere-2025-5433
Preprint. Discussion started: 18 November 2025

This seasonal connectivity markedly affects the lake's water level and surface area. In a typical hydrological year, the water level fluctuation in HWL between wet and dry seasons can reach 8 m.

The aquifer interacting with the oxbow lake comprises two distinct layers (Figure 1c). The upper layer with 5–15 m thickness consists of low-permeability clay and silty clay with a hydraulic conductivity of approximately 1 $m \cdot d^{-1}$. In contrast, the lower layer is a confined aquifer 50–80 m thick, composed mainly of fine to coarse sand, and exhibits a higher hydraulic conductivity of approximately 5–15 $m \cdot d^{-1}$. Owing to its greater permeability, the lower aquifer functions as the primary groundwater source directly connected to the lake. Previous studies have confirmed substantial LGD in HWL, predominantly occurring as springs (Figure 1 d1–d6) and seepage flows.

In 2022, a severe drought event in YR caused the water level of HWL to decline in parallel with that of the YR, ultimately leading to complete disconnection from the river. Consequently, the lake entered the dry season approximately two months earlier than that in a typical hydrological year. During the groundwater discharge period, the water level of HWL was minimally affected by hydrological fluctuations in the YR and was instead primarily controlled by meteorological factors such as precipitation and evaporation.

https://doi.org/10.5194/egusphere-2025-5433
Preprint. Discussion started: 18 November 2025

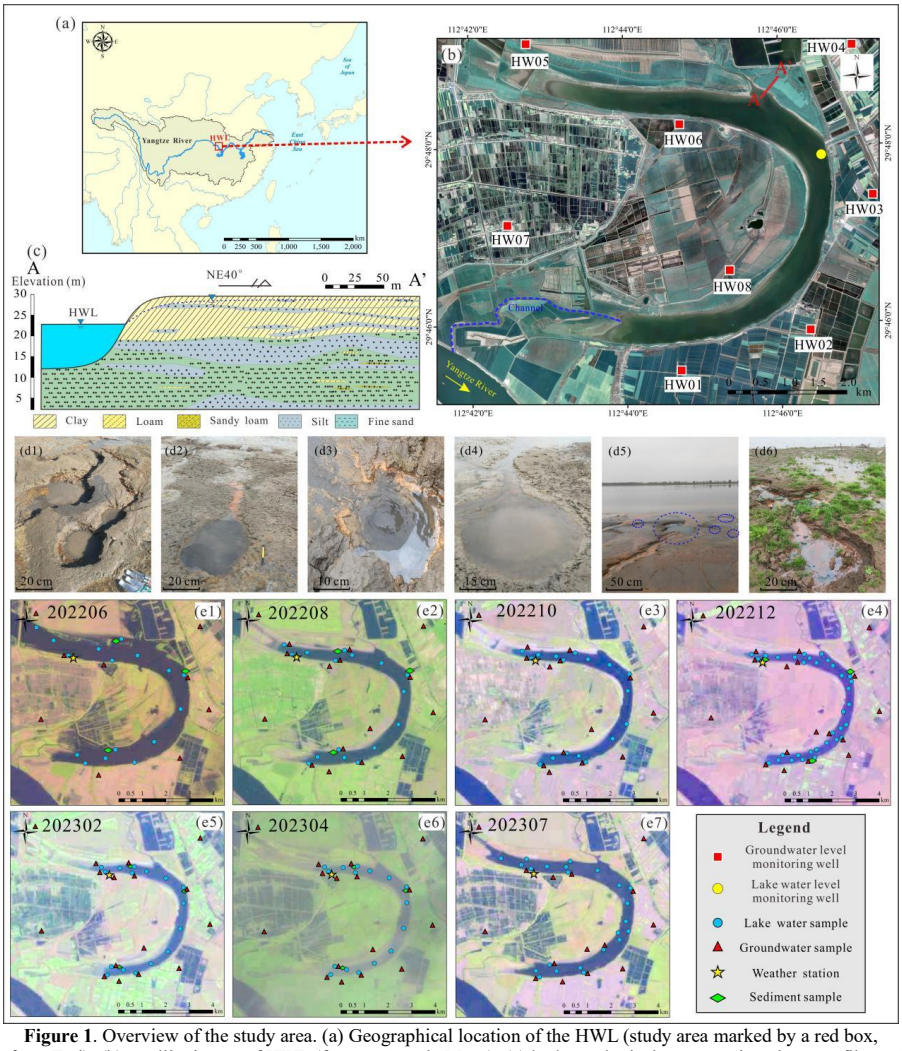

Figure 1. Overview of the study area. (a) Geographical location of the HWL (study area marked by a red box, from Esri); (b) satellite image of HWL (from © Google Maps); (c) hydrogeological cross-section along profile A–A' (profile location indicated by line A–A' in b). (d1–d6) Zones of concentrated LGD phenomena in HWL, primarily manifested as spring outlets; (e1–e7) spatial distribution of field sampling sites collected between June and July 2022 (from Landsat 8). The numbers in the figure indicate the sampling periods. For example, 202208 represents August 2022.

2.2 Field work and laboratory analysis

Systematic field sampling was conducted from June 2022 to July 2023, with a sampling frequency of once every two months. Except for the July 2023 sampling conducted in early July, all other campaigns were performed at the end of the even-numbered months. Except for the campaigns in June 2022, December 2022, and July 2023, all sessions followed a standardized protocol involving the collection of 16 lake water samples, 8 well water samples, and 8 spring water (pore water) samples. A

https://doi.org/10.5194/egusphere-2025-5433
Preprint. Discussion started: 18 November 2025

total of 241 samples were collected (Table 1, Figure 1 e1–e7), comprising 135 lake water samples, 56 well water samples, and 50 pore water samples. In addition to sample collection, each campaign included simultaneous measurements of environmental parameters, such as groundwater level, lake water level, lake depth, and wind speed. Due to seasonal fluctuations in lake water levels, the shoreline position shifted over time, resulting in slight spatial variations in the lakeshore sampling points across campaigns. The wind speed was continuously recorded at 15-min intervals using a weather station installed on the lakeshore, while the precipitation and evaporation data were sourced from the ECMWF reanalysis datasets.

Table 1. Number of samples per sampling campaign.

Time	Number of lake water samples	Number of well water samples	Number of pore/spring water samples	Total
June 23–29, 2022	16	8	2	26
August 26–30, 2022	16	8	8	32
October 26–31, 2022	16	8	8	32
December 17–30, 2022	35	8	10	53
February 20–25, 2023	16	8	8	32
April 23–27, 2023	16	8	8	32
July 6–14, 2023	20	8	6	34
Total	135	56	50	241

Samples from the lake center were collected by boat at fixed preselected locations. Surface water was sampled approximately 0.5 m below the surface using a specialized surface water sampler. The groundwater samples were categorized into two types: (1) well water collected from monitoring wells located 0.5 to 2.5 km from the lakeshore, with the depths between 15 and 30 m, and (2) spring water collected from natural springs situated within 15 m of the shoreline and in shallow lake zones, serving as the representative lakeshore pore water. In addition, three nearshore lakebed sediment samples were collected for incubation experiments to determine the ^{222}Rn concentrations. The wind speed was continuously recorded at 15-min intervals using a weather station installed on the lakeshore, while the precipitation and evaporation data were sourced from the ECMWF reanalysis datasets.

Water quality parameters, including pH, temperature, DO, ORP, and EC, were measured in situ using a HACH-HQ40D multi-parameter probe. Chl *a* concentrations were determined immediately after sampling using an AquaFluor fluorometer, with a detection limit of 0.5 $\mu g \cdot L^{-1}$. For ^{222}Rn analysis, the water samples were collected in 250 mL or 2.5 L glass bottles using an overflow method to eliminate residual air. ^{222}Rn concentrations were quantified using a RAD7 system (Durridge Company,

https://doi.org/10.5194/egusphere-2025-5433
Preprint. Discussion started: 18 November 2025

Inc.) equipped with RAD7-H_2O and RAD7 Big Bottle accessories. To reduce the measurement uncertainty in the lake water samples, the counting time was extended to 60 min per sample. All ^{222}Rn analyses were completed within 24 h of sampling, using the RAD7 aqueous system.

$$A_0 = A \times e^{\lambda t} \quad (1)$$

where A_0 represents the ^{222}Rn concentration ($Bq \cdot m^{-3}$) at the sampling time; A represents the ^{222}Rn concentration ($Bq \cdot m^{-3}$) at the measurement time; λ represents the decay coefficient of ^{222}Rn, 0.181 d^{-1}; and t represents the time interval (d) between sampling and measurement. The uncertainty in ^{222}Rn testing for lake water was approximately 35%, and the uncertainty in ^{222}Rn testing for groundwater is approximately 25%.

The samples for total nitrogen (TN) and total phosphorus (TP) analysis were field-filtered using a 0.45 μm membrane filter and then stored in 30 mL polyethylene bottles and 20 mL brown screw-cap glass bottles, respectively. The TP samples were acidified with concentrated HNO_3 to a pH below 2, sealed, and subsequently analyzed using an inductively coupled plasma optical emission spectrometer (ICP-OES, iCAP 6000 series, Thermo Fisher Scientific, USA) at the School of Environmental Studies, China University of Geosciences (Wuhan), with a detection limit of 0.001 $mg \cdot L^{-1}$. TN samples were analyzed using a total organic carbon/nitrogen analyzer at the Wuhan Botanical Garden, Chinese Academy of Sciences, with a detection limit of 0.01 $mg \cdot L^{-1}$.

2.3. ^{222}Rn mass balance model

In recent years, ^{222}Rn has been widely used in studies of LGD. Derived from its parent isotope ^{226}Ra, ^{222}Rn has a half-life of 3.82 d. By treating lake water as a closed system, a mass balance model was developed based on both the sources and sinks of ^{222}Rn. The ^{222}Rn flux from the groundwater discharge was inferred as an unknown term. The ^{222}Rn mass balance model is expressed as follows:

$$\frac{\partial I^{222}Rn}{\partial t} = F_g + F_d + I^{226}Ra \times \lambda^{226}\mathrm{Ra} - F_a - I^{222}Rn \times \lambda^{222}Rn \quad (2)$$

where F_g, F_d, and F_a are the ^{222}Rn fluxes ($Bq \cdot m^{-2} \cdot d^{-1}$) of groundwater discharge, sediment diffusion, and atmospheric escape, respectively; $I^{226}Ra$ and $I^{222}Rn$ are the pools of ^{226}Ra and ^{222}Rn in the lake water ($Bq \cdot m^{-2}$), which are equal to the concentrations of ^{226}Ra and ^{222}Rn multiplied by the water depth; and

https://doi.org/10.5194/egusphere-2025-5433
Preprint. Discussion started: 18 November 2025

the decay coefficients of ^{222}Rn ($\lambda^{222}Rn$) and ^{226}Ra ($\lambda^{226}Ra$) were 0.181 d^{-1} and 1.31 × 10^{-11} d^{-1}, respectively.

The LGD rate can be obtained by dividing the ^{222}Rn flux from groundwater discharge by the ^{222}Rn concentration of surrounding groundwater. The formula is as follows (Luo et al., 2018; Wang et al., 2019):

$$V = \frac{F_g}{C_g} \times 1000 \quad (3)$$

where V is the average LGD rate ($mm \cdot d^{-1}$); Fg is the ^{222}Rn flux of groundwater discharge ($Bq \cdot m^{-2} \cdot d^{-1}$) ; Cg is the ^{222}Rn concentrations in groundwater end member ($Bq \cdot m^{-3}$). A more detailed description can be found in Section 1 of the SI.

3 Results and Discussion

3.1 Seasonal variations in LGD rates

3.1.1 Identification of seasonal variations in LGD

1. Lake water and groundwater level

From June 2022 to July 2023, the lake water level fluctuated significantly between 22.30 and 32.90 m, with a peak in late June 2022 and a low in late February 2023, demonstrating a variation of 10.6 m (Figure 2a). Initially, the HWL's high water level was sustained by its connection to the Yangtze River, which was at a high level in June 2022. However, a severe drought from August to September 2022 caused a rapid decline in the Yangtze River level, resulting in a corresponding decrease in the HWL level. From late October 2022 to early May 2023, as the Yangtze River fell below 26.5 m, HWL became hydrologically isolated, with no surface water inflow or outflow. The rate of water level decline slowed from October 2022 to February 2023 and began to rise in March 2023 because of increased precipitation. In May 2023, when the Yangtze River exceeded 26.5 m again, the HWL level rose sharply due to the inflow.

The groundwater levels from the eight surrounding wells exhibited similar fluctuations, ranging from 26.6 to 30.9 m (Figure 2a). From June 2022 to April 2023, groundwater levels consistently declined, with a slight increase observed from April to July 2023. Generally, the groundwater level trends mirrored those of the lake, except for the period from February to April 2023, when the groundwater levels decreased while the lake levels increased. The difference between the average

https://doi.org/10.5194/egusphere-2025-5433
Preprint. Discussion started: 18 November 2025

groundwater and lake levels ranged from -1.98 to 4.45 m, affecting the LGD rates over time. In June 2022, all eight wells had groundwater levels lower than those of the lake, indicating complete lake recharge. By July 2023, four wells presented lower groundwater levels, whereas four exhibited higher levels, suggesting simultaneous recharge and discharge. From August 2022 to April 2023, groundwater consistently discharged into the lake, with the largest groundwater-lake level difference occurring in December 2022, indicating the highest LGD rate during that period (Figure 2b).

2. Lake water and groundwater ^{222}Rn concentration

The fluctuation in the lake water ^{222}Rn concentration from June 2022 to July 2023 (Figure 2c) exhibited an initial increase followed by a decrease. The lowest concentration occurred in June 2022, whereas the highest was recorded in December 2022, with values of 87.50 and 231.61 $Bq \cdot m^{-3}$, respectively. Similarly, groundwater also demonstrated a trend of initial decrease followed by an increase (Figure 2d), with the highest values in June 2022 and the lowest values in April 2023, at 5863.45 and 2558.30 $Bq \cdot m^{-3}$ respectively.

During the period of groundwater discharge to the lake, when groundwater levels were consistently above lake levels (August 2022 to April 2023), the lake water ^{222}Rn concentration ranged from 106.83 to 231.61 $Bq \cdot m^{-3}$. While, the groundwater ^{222}Rn concentration ranged from 2558.30 to 3910.40 $Bq \cdot m^{-3}$. Based on the coefficient of variation (CV), the ^{222}Rn concentration in groundwater ($CV \approx 17.60\%$) is more stable than that in lake water ($CV \approx 26.62\%$), indicating a relatively consistent ^{222}Rn endmember value for groundwater. Because groundwater was the primary source of ^{222}Rn in the lake, variations in lake water ^{222}Rn concentrations reflected changes in the LGD rate. As shown in Figure 2e, the ratio of lake water to groundwater ^{222}Rn concentration initially increased and then decreased with a peak in December 2022, which suggested that the LGD rate was the highest during that period. This pattern is consistent with the relationship between groundwater and lake water levels.

https://doi.org/10.5194/egusphere-2025-5433
Preprint. Discussion started: 18 November 2025

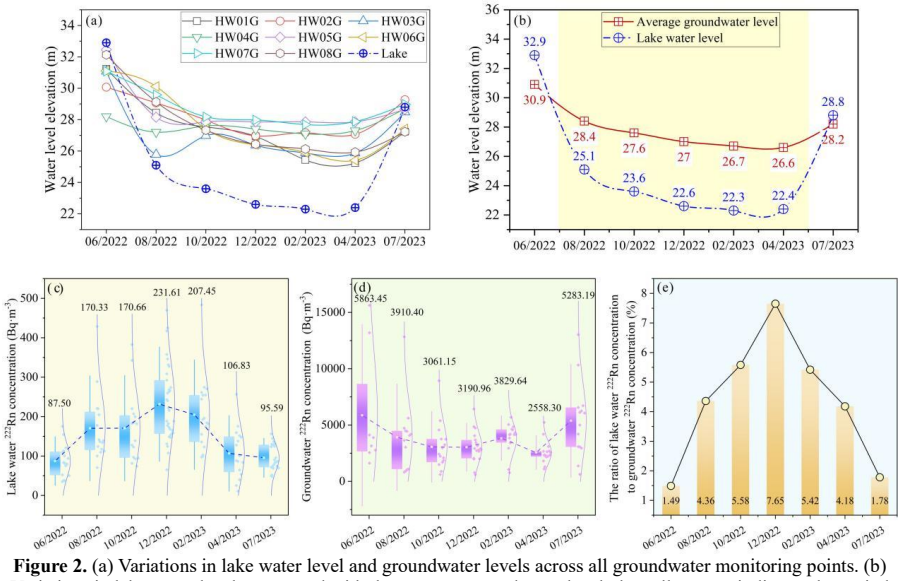

Figure 2. (a) Variations in lake water level and groundwater levels across all groundwater monitoring points. (b) Variations in lake water levels compared with the average groundwater level, the yellow area indicates the period of LGD. (c) Variations in the lake water concentrations of ^{222}Rn. (d) Variations in the groundwater concentrations of ^{222}Rn. (e) Variations in the ratio of ^{222}Rn concentrations in lake water to groundwater.

3.1.2 Quantification of LGD rates for each period

Based on the lake level and groundwater monitoring data, the period from late August 2022 to late April 2023 was characterized by consistently higher groundwater levels than the lake stage, during which the lake was hydrologically isolated from external surface water inputs. This interval was conservatively defined as the active phase of LGD (Figure 2b). Using the ^{222}Rn mass balance model, LGD rates were computed for each period of groundwater discharge during groundwater excretion.

Table 2 summarizes the detailed parameters and results for the source and sink terms across each sampling period. In terms of source, the groundwater-derived ^{222}Rn input flux ranged from 90.48 ± 36.32 to 165.02 ± 63.09 Bq·m^{-2}·d^{-1}, while the diffusive flux of ^{222}Rn from sediment pore water varied between 18.82 ± 2.88 and 21.51 ± 3.29 Bq·m^{-2}·d^{-1}. In terms of sink, the radioactive decay flux of ^{222}Rn in lake water ranged from 73.47 ± 26.74 to 163.49 ± 59.51 Bq·m^{-2}·d^{-1}, and atmospheric evasion accounted for a flux of 20.34 ± 6.46 to 38.51 ± 12.87 Bq·m^{-2}·d^{-1}.

The LGD rates for each period were calculated by dividing the flux of ^{222}Rn input from LGD by the corresponding groundwater ^{222}Rn concentration (Figure 3a). From August 2022 to April 2023, the LGD rates ranged from 35.36 ± 16.39 to 51.71 ± 23.23 mm·d^{-1}, with the maximum value being 1.46 times the minimum value. Notably, an increasing trend in groundwater excretion rates was observed

https://doi.org/10.5194/egusphere-2025-5433
Preprint. Discussion started: 18 November 2025

from August 2022 to December 2022, which was followed by a decreasing trend from December 2022 to April 2023. The highest rate of groundwater excretion occurred in December 2022, whereas the lowest LGD rate was recorded in April 2023.

Table 2. The calculation parameters and results of the ^{222}Rn mass balance model for each period.

	08/2022	10/2022	12/2022	02/2023	04/2023
Lake water ^{222}Rn concentration ($Bq \cdot m^{-3}$)	170.33 ± 88.71	170.66 ± 89.10	231.61± 96.53	207.45±98.16	106.83±63.85
Air ^{222}Rn concentration ($Bq \cdot m^{-3}$)	16.20	16.20	16.20	16.20	16.20
Wind speed above 2 m lake surface ($m \cdot s^{-1}$)	1.48±0.82	1.37±0.83	1.08±1.11	1.65±1.44	2.05±1.57
K ($m \cdot d^{-1}$)	0.30±0.02	0.17±0.01	0.08±0.01	0.16±0.01	0.34±0.01
Sc	554.34	937.71	1572.2	1492.73	871.45
Lake water temperature (°C)	29.19	18.43	8.86	9.78	19.89
Lake water depth (m)	4.9	4.2	3.9	3.8	3.8
Groundwater ^{222}Rnconcentration ($Bq \cdot m^{-3}$)	3910.40 ± 3511.38	3061.15± 2099.00	3028.17± 1412.72	3829.64± 1316.67	2588.30± 998.11
The ^{222}Rn flux of atmospheric escape ($Bq \cdot m^{-2} \cdot d^{-1}$)	49.80±18.20	30.96±10.27	20.34±6.46	37.12±11.56	38.51±12.87
The ^{222}Rn flux of pore in sediment diffusion ($Bq \cdot m^{-2} \cdot d^{-1}$)	24.70±3.78	21.10 ± 3.23	18.82±2.88	18.74±2.87	21.51±3.29
The ^{222}Rn flux of decay ($Bq \cdot m^{-2} \cdot d^{-1}$)	151.07± 54.99	129.74±47.22	163.49±59.51	142.68±51.93	73.47±26.74
The ^{222}Rn flux of groundwater discharge ($Bq \cdot m^{-2} \cdot d^{-1}$)	176.16± 58.05	139.59±48.44	165.02± 63.09	161.06±60.63	90.48±36.32
LGDrate ($mm \cdot d^{-1}$)	45.05± 18.39	45.60± 34.20	51.71±23.23	42.06±18.60	35.36±16.39

3.2 Climatic controls on seasonal variations in LGD rates

3.2.1 Relationship between precipitation and evaporation and LGD rates

To obtain a higher temporal resolution within the hydrological year, fitting equations were established to simulate the monthly LGD rates during groundwater discharge periods. The quadratic equation representing LGD rates based on the ^{222}Rn mass balance model and time was $Y = -0.54X^2 + 6.42X + 29.82$, $R^2 = 0.83$, $P < 0.05$ (where X represents the time and Y represents the LGD rate) (Figure 3a). Using this equation, the LGD rates were estimated for the period from August 2022 to May 2023. Although the water level at the Jianli station of the Yangtze River exceeded 26.5 m in May 2023 for just 10 d, the inflow from the Yangtze River to the HWL was minimal and insufficient to raise the lake level above the groundwater level. Therefore, groundwater discharge into the lake continued in May 2023. The simulated LGD rates ranged from 35.10 to 48.90 $mm \cdot d^{-1}$ between August 2022 and

https://doi.org/10.5194/egusphere-2025-5433
Preprint. Discussion started: 18 November 2025

May 2023 (Figure 3b), with an approximately 8% error compared to the rates derived from the ^{222}Rn mass balance model. These rates exhibited an increasing trend followed by a decreasing trend, peaking in the middle of the groundwater discharge period, and tapering at both the beginning and end stages.

During the groundwater discharge period, the changes in precipitation and evaporation were inversely related to the changes in LGD, demonstrating a clear negative correlation with LGD rates, with correlation coefficients of R^2=0.61, P < 0.01 and R^2=0.67, P < 0.01, respectively (Figure 3b). This suggested that lower monthly precipitation and evaporation contributed to the larger LGD. This aligns with Jiang et al.'s (2024) results showing an inverse relationship between LGD rates and precipitation/evaporation. Additionally, the value of precipitation minus evaporation (PME) played a significant role in the hydrological cycle. By analyzing the relationship between the PME and LGD rates, a non-linear relationship was identified, with the fitted equation being $Y=-0.0004X^2-0.0139X+47.08$, R^2=0.86, P<0.05 (Figure 3c). When PME was greater than 0, a larger PME resulted in a smaller LGD. When PME was less than 0, a smaller PME led to a smaller LGD. When both precipitation and evaporation were low and the PME approached 0, LGD reached its maximum value.

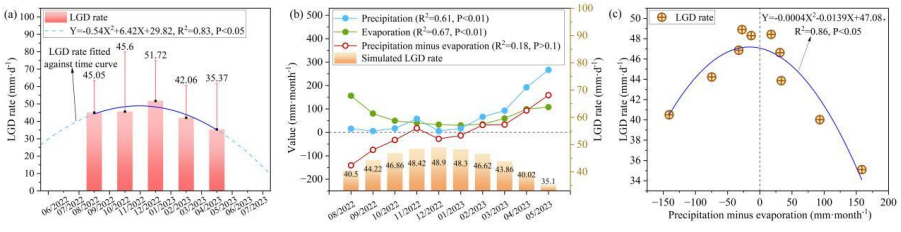

Figure 3. (a) The LGD rate of different periods and their fitted relationship between LGD rate and time. (b) Relationship between simulated LGD rate and precipitation and evaporation, where R^2 represents the linear correlation coefficient between this indicator and the LGD rate. (c) Relationship between PME and LGD rate.

3.3.2 Dominance of precipitation and evaporation on seasonal variations in LGD rates

At different periods, a strong correlation was observed between the LGD rate and hydraulic gradient (R^2=0.77, P<0.05) (Figure 4a), with both showing a consistent trend of change, in accordance with Darcy's law (Tecklenburg and Blume; 2017) (Figure 4a). The hydraulic gradient is controlled by the water level difference between groundwater and lake water—when this difference increases, the LGD rate rises; when it decreases, the LGD rate declines. From August to December 2022, the water level difference increased, leading to a rising LGD rate; from December 2022 to April 2023, the difference decreased, resulting in a lower LGD rate (Figure 4a). This variation is determined by the

https://doi.org/10.5194/egusphere-2025-5433
Preprint. Discussion started: 18 November 2025

differences in groundwater level and lake water level. If the lake level drops more than the groundwater level, the gradient increases and LGD intensifies; if the groundwater level drops more, the gradient and LGD both decline (Figure 4b).

Monitoring data show that lake levels consistently declined during the study period, though the rate of decline slowed, primarily due to low precipitation, reduced evaporation, cooler temperatures, and decreased water consumption by agriculture and aquatic organisms. After February 2023, increasing precipitation slightly raised lake levels. Groundwater levels also declined steadily, mainly due to continuous LGD to lake, with minimal influence from human extraction or evaporation. Between August and December 2022, groundwater levels fell more slowly than lake levels, increasing the hydraulic gradient and LGD. From February 2023 onward, the groundwater level declined more than the lake level, reducing the gradient and LGD rate. By April 2023, groundwater levels stabilized while lake levels rose slightly, further decreasing the hydraulic gradient and LGD.

Net precipitation (PME) directly affects lake level fluctuations and indirectly influences groundwater levels by altering the water level difference (Figure 4c). A higher PME slows or reverses lake level decline, reducing groundwater discharge and limiting groundwater level drop. A lower PME accelerates lake level decline, enhancing groundwater discharge and deepening the groundwater level drop. Therefore, PME modulated the lake level changes, which subsequently influenced the groundwater levels, altered the lake-groundwater level difference, and regulated the hydraulic gradient, ultimately controlling the seasonal variations in LGD rates.

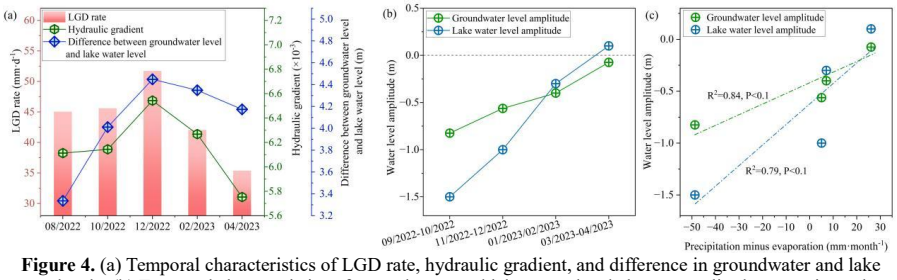

Figure 4. (a) Temporal characteristics of LGD rate, hydraulic gradient, and difference in groundwater and lake water levels. (b) Temporal characteristics of groundwater and lake water level change amplitudes, negative values indicate the amplitudes of water level decline, while positive values represent the amplitudes of water level rise. (c) Relationship between groundwater level amplitude, lake water level amplitude, and PME.

3.3 Impact of LGD-carried N and P on seasonal nutrient status of lakes

3.3.1 Seasonal variations in TN and TP loads carried by LGD

Between August 2022 and April 2023, the concentration of TN in the groundwater exhibited notable temporal variability, ranging from 0.24 to 0.46 mmol·L^{-1}. The lowest concentration was

https://doi.org/10.5194/egusphere-2025-5433
Preprint. Discussion started: 18 November 2025

observed in August 2022, whereas the peak was observed in December 2022 (Table 3). In comparison, the range of temporal variations in TP concentration in groundwater was wider, spanning from 6.46 × 10^{-3} to 2.19 × 10^{-2} mmol·L^{-1} (Table 3). The lowest TP concentration was recorded in December 2022, whereas the highest occurred in February 2023. These fluctuations in TN and TP concentrations in the groundwater were irregular. Such variations could be due to changes in groundwater levels, which affected the redox conditions, microbial communities, and biogeochemical processes, thus influencing the intensity of N and P release from aquifer sediments into groundwater.

Table 3. Concentrations of TN and TP in groundwater at various periods and loads of TN and TP carried by LGD.

	TN concentration in groundwater (mmol·L^{-1})	TP concentration in groundwater (mmol·L^{-1})	LGD-TN (mmol·m^{-2}·d^{-1})	LGD-TP (mmol·m^{-2}·d^{-1})
08/2022	0.24	1.69×10^{-2}	10.76	0.76
10/2022	0.33	2.00×10^{-2}	15.22	0.91
12/2022	0.46	6.46×10^{-3}	24.00	0.33
02/2023	0.34	2.19×10^{-2}	14.25	0.92
04/2023	0.39	8.24×10^{-3}	13.93	0.29

Multiplying the LGD rate by the concentrations of TN and TP in the groundwater demonstrated the nutrient load carried by LGD. The variations in nutrient loads from August 2022 to April 2023 are shown in Figures 4d and 4e. The loads of TN carried by LGD (LGD-TN) ranged from 10.76 to 24.00 mmol·m^{-2}·d^{-1}, with the lowest load occurring in August 2022 and the highest in December 2022. Similarly, the loads of TP carried by LGD (LGD-TP) ranged from 0.29 to 0.92 mmol·m^{-2}·d^{-1}, with the highest load observed in December 2022 and the lowest in April 2023. The temporal variation in LGD-TN loads followed the trend of the LGD rate and was primarily influenced by the LGD rate. In contrast, the variation in LGD-TP loads over time did not align with the LGD rate and was mainly controlled by the concentration of TP in the groundwater.

3.3.2 Seasonal relationship between LGD-carried TN/TP loads and nutrient status of lakes

The nutrient status of lakes is determined by various parameters, and the concentration of Chl *a* in lake water is considered particularly important. In this study, no significant correlation was observed between Chl *a* concentration and the concentrations of TN and TP (Figures 5a and 5b). However, a correlation was identified with the TN to TP molar ratio (TN/TP) (Figure 5c). As the TN/TP ratio approached the Redfield ratio of 16 (Figure 5c), the Chl *a* concentration increased (AC, 1960), whereas a deviation from this ratio was associated with a decrease in Chl *a* concentration, which was consistent with the findings reported in other studies (Qin et al., 2020).

https://doi.org/10.5194/egusphere-2025-5433
Preprint. Discussion started: 18 November 2025

In the absence of surface water inflow and pollutant discharge from prohibited human activities, N and P enter the lake primarily through groundwater discharge, atmospheric deposition, and sediment release. To quantify TN and TP inputs from atmospheric deposition and sediment release, comprehensive field monitoring and experimental investigations were conducted during HWL periods (Tables S1 and S2). The results indicated that the TN and TP loads from atmospheric deposition were 0.09 and 9.68×10^{-4} mmol·m^{-2}·d^{-1}, respectively. Simultaneously, the diffusive TN and TP loads from lakebed sediment were 0.08 and 1.29×10^{-4} mmol·m^{-2}·d^{-1}, respectively. In contrast, the LGD-TN and LGD-TP loads were 1–2 orders of magnitude higher than those from atmospheric deposition and sediment release, indicating that LGD-TN and LGD-TP constituted the primary sources of TN and TP in the lake. A strong correlation was observed between LGD-TN loads and TN concentrations in lake water (R^2=0.79, P<0.05) (Figure 5d), whereas the LGD-TP loads exhibited entirely consistent variations with TP concentrations in lake water (R^2=0.89, P<0.05) (Figure 5e), highlighting their significant influence.

The molar ratio of TN to TP in LGD (LGD-TN/TP) exhibited variations that were entirely consistent with the TN/TP ratio in the lake water, indicating a strong correlation (R^2=0.82, P<0.05) (Figure 5f), thereby indicating its regulatory effect on the lake water TN/TP ratio. Based on the observed changes in LGD-TN/TP and their reflection in lake water TN/TP, when the lake water TN/TP reached 15.35 in April 2023, the Chl *a* concentration was elevated. These results demonstrated that the LGD-derived TN and TP substantially influenced the lake's nutrient status by modulating the TN/TP ratio, thereby affecting the Chl *a* concentration and the overall nutrient balance.

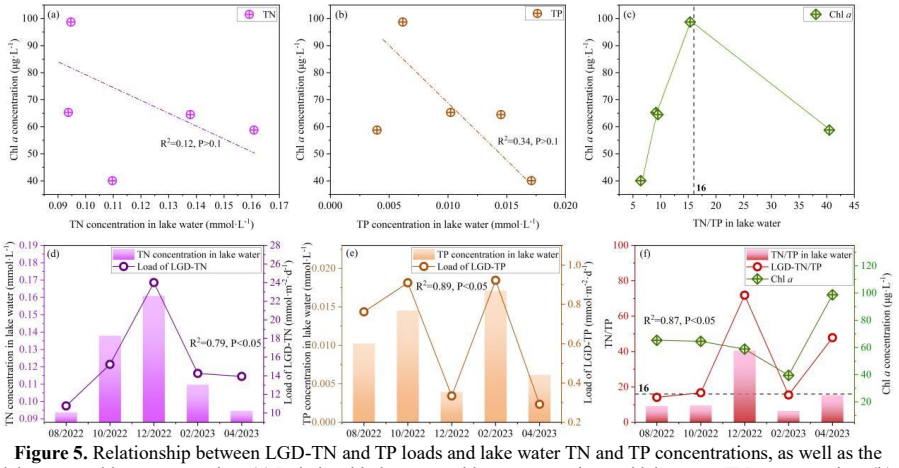

Figure 5. Relationship between LGD-TN and TP loads and lake water TN and TP concentrations, as well as the lake water Chl *a* concentration. (a) Relationship between Chl *a* concentration and lake water TN concentration. (b) Relationship between Chl *a* concentration and lake water TP concentration. (c) Relationship between Chl *a*

https://doi.org/10.5194/egusphere-2025-5433
Preprint. Discussion started: 18 November 2025

concentration and lake water TN/TP. (d) Relationship between lake water TN concentration and LGD-TN load. (e) Relationship between lake water TP concentration and LGD-TP load. (f) Relationship between lake water TN/TP and LGD-TN/TP load.

3.4 Implications

3.4.1 Dominant factors controlling the seasonal variability of LGD

The seasonal variability of LGD is primarily governed by three categories of factors—meteorological, hydrological, and anthropogenic—with the dominant controls differing across lake types.

(1) In open lakes (e.g., Poyang Lake and Tonle Sap Lake), hydrological processes dominate LGD dynamics. Their hydraulic connection with external rivers (such as the Yangtze and Mekong Rivers) causes rapid lake-level rises during the wet season and pronounced declines during the dry season, thereby modifying the hydraulic gradients between the littoral zone and aquifer and directly regulating groundwater discharge rates (Burnett et al. 2017; Li et al. 2020). (2) In closed lakes, where external fluvial influence is minimal, LGD dynamics are primarily controlled by the balance between precipitation and evaporation. Previous studies (Shi et al., 2022; Gan et al., 2024) have shown that under relatively stable groundwater levels, strong evaporation lowers lake levels, steepens the hydraulic gradient, and enhances LGD, whereas precipitation-dominated periods raise lake levels and suppress LGD. Hence, the seasonal oscillation of LGD in closed-basin systems essentially reflects a periodic adjustment of lake–groundwater hydraulic connectivity driven by meteorological forcing. (3) Anthropogenic activities, such as artificial water regulation and groundwater abstraction, can further modify LGD by altering regional hydrological circulation and the hydraulic relationships between lakes and aquifers (Xiong et al., 2023).

3.4.2 Regulatory role of LGD in lake nutrient status

In closed lakes lacking significant surface inflow, LGD not only constitutes a key component of the water balance but also plays a pivotal role in nutrient transport and water quality evolution. The nitrogen and phosphorus fluxes carried by LGD directly influence the spatial and temporal patterns of nutrient concentrations and chlorophyll-a within the lake. Several studies support this mechanism. For instance, Xu et al. (2024) showed that in small semi-arid lakes, LGD inputs largely determine the spatial distribution of chl *a*, while Shi et al. (2022) reported a delayed response of lake trophic

https://doi.org/10.5194/egusphere-2025-5433
Preprint. Discussion started: 18 November 2025

conditions to LGD-derived nutrient inputs. Such lakes are typically characterized by strong enclosure and long water residence times, conditions that amplify the influence of groundwater in biogeochemical cycling and ecological processes.

Synthesizing current knowledge, the linkage from seasonal forcing to ecological response in closed lakes can be conceptualized as follows: meteorological conditions (precipitation–evaporation balance) serve as the initial driver, regulating lake–groundwater hydraulic gradients and thereby controlling the seasonal magnitude of LGD. LGD, in turn, acts as a key conduit for nutrient fluxes, with its temporal variability shaping nutrient and chl *a* distributions and ultimately modulating nutrient dynamics. Although comprehensive case studies remain scarce, existing evidence indicates that LGD is likely a critical mechanism underpinning nutrient cycling and ecological succession in closed lakes, meriting systematic and in-depth investigation in future research.

4 Conclusions

High-frequency monitoring and hydrochemical methods were employed to investigate the dynamics of LGD and associated nutrient loads in Heiwawu Oxbow Lake from August 2022 to April 2023, revealing the regulatory mechanisms of precipitation-evaporation processes. The LGD flux exhibited an increasing-then-decreasing trend during the study period, ranging from 35.36 to 51.71 $mm \cdot d^{-1}$, with a peak in December 2022 and a minimum in April 2023. The LGD rates were governed by the hydraulic gradient between groundwater and lake water, which responded nonlinearly to net monthly precipitation. Positive net precipitation induced rapid lake recharge, reduced the hydraulic gradient, and suppressed LGD rates. Conversely, negative net precipitation enhanced evaporation-driven lake discharge, steepened the hydraulic gradient, and increased LGD rates. When net precipitation approached zero, a critical hydraulic equilibrium was reached, yielding the highest LGD rates. The LGD was also a major nutrient pathway, with TN and TP loads significantly correlating with lake concentrations. The TN/TP ratio of LGD aligned with lake water, influencing phytoplankton structure and Chl a levels. This study elucidates the monthly-scale regulatory mechanism of precipitation-evaporation balance on LGD and to quantitatively assess the role of groundwater-driven nutrient transport in lake eutrophication. These findings offer a novel perspective for managing eutrophication in closed shallow lakes, and the incorporation of LGD monitoring into lake management frameworks is recommended, along with the development of targeted control strategies for critical

https://doi.org/10.5194/egusphere-2025-5433
Preprint. Discussion started: 18 November 2025

periods of groundwater-lake interactions.

Acknowledgments

The research was funded by National Natural Science Foundation of China (No. U21A2026), Project of Hubei Provincial Key Research and Development (No. 2022BCA074), and Natural Science Foundation of Hubei Province (2022CFA029). The authors would like to thank all the reviewers who participated in the review.

Declaration of interests

The authors declare that they have no known competing financial interests or personal relationships.

Data Availability Statement

Data will be made available on request.

Author contributions

Writing-review & editing, Writing-original draft, Methodology, Investigation, Data curation: XS. Writing-review & editing, Resources, Methodology, Funding acquisition: YD. Investigation: HT, JX, HS, YL. Project administration: YD. Funding acquisition: YG. Resources, Project administration: YW.

References

AC, R. (1960). The biological control of chemical factors in the environment. Science progress, 11, 150–170.

Adyasari, D., Dimova, N. T., Dulai, H., Gilfedder, B. S., Cartwright, I., McKenzie, T., & Fuleky, P. (2023). Radon-222 as a groundwater discharge tracer to surface waters. Earth-Science Reviews, 104321.

Burnett, W. C., Wattayakorn, G., Supcharoen, R., Sioudom, K., Kum, V., Chanyotha, S., & Kritsananuwat, R. (2017). Groundwater discharge and phosphorus dynamics in a flood-pulse system: Tonle Sap Lake, Cambodia. Journal of Hydrology, 549, 79–91.

Dabrowski, J. S., Charette, M. A., Mann, P. J., Ludwig, S. M., Natali, S. M., Holmes, R. M., & Henderson, P. B. (2020). Using radon to quantify groundwater discharge and methane fluxes to a

https://doi.org/10.5194/egusphere-2025-5433
Preprint. Discussion started: 18 November 2025

shallow, tundra lake on the Yukon-Kuskokwim Delta, Alaska. Biogeochemistry, 148, 69–89.

Du, Y., Deng, Y., Ma, T., Shen, S., Lu, Z., & Gan, Y. (2020). Spatial variability of nitrate and ammonium in Pleistocene aquifer of central Yangtze River Basin. Groundwater, 58(1), 110–118.

Gan, Y., Sun, X., Wu, J., Du, Y., Deng, Y., Han, P., & Wang, Y. (2024). Spatio-temporal variations of lacustrine groundwater discharge and related nutrient fluxes in a typical lake in front of hillocks. Journal of Hydrology, 635, 131166.

Gao, X., Jia, T., Xu, Q., Wang, F., & Wang, A. (2016). Records of lacustrine sedimentology and pollen-charcoal assemblages responding to climate change and human activities in Zhongzhouzi Oxbow Lake, Hubei Province for about 70 years. Quaternary Sciences, 36(6), 1445–1455.

Hu, M., Zhou, P., & Chen, C. (2023). Study on coupling of typical elements in surface water and groundwater in the middle reaches of the Yangtze River, China. Journal of Hydrology, 130298.

Jia, T., Wang, F., & Yuan, S. (2015). Sedimentation and its environmental significance of the Niuyu Lake along the middle reaches of the Yangtze River: A case study of Tian'e Island and Zhongzhouzi in the Jingjiang section of the Yangtze River. Geographical Research, 34(05), 861–871. (in chinese)

Jiang, C., Jiang, C., Wang, Q., Liu, H., Li, D., Zhu, Q., & Liu, F. (2024). Seasonal characteristics of groundwater discharge controlled by precipitation and its environmental effects in a coal mining subsidence lake, eastern China. Science of The Total Environment, 915, 170067.

Jiang, X., Ma, R., Ma, T., & Sun, Z. (2022). Modeling the effects of water diversion projects on surface water and groundwater interactions in the central Yangtze River basin. Science of the Total Environment, 830, 154606.

Kazmierczak, J., Postma, D., Muller, S., Jessen, S., Nilsson, B., Czekaj, J., & Engesgaard, P. (2020). Groundwater-controlled phosphorus release and transport from sandy aquifer into lake. Limnology And Oceanography, 11447.

Kluge, T., Ilmberger, J., Von Rohden, C., & Aeschbach-Hertig, W. (2007). Tracing and quantifying groundwater inflow into lakes using a simple method for radon-222 analysis. Hydrology and Earth System Sciences, 11(5), 1621–1631.

Lewandowski, J., Rosenberry, D.O., & Meinikmann, K. (2024). Groundwater–Lake Interfaces. Ecohydrological Interfaces, 103–122.

Luo, X., Kuang, X.X., Jiao, J.J., Liang, S.H., Mao, R., Zhang, X.L., & Li, H.L. (2018), Evaluation of

https://doi.org/10.5194/egusphere-2025-5433
Preprint. Discussion started: 18 November 2025

lacustrine groundwater discharge, hydrologic partitioning, and nutrient budgets in a proglacial lake in the Qinghai-Tibet Plateau: using ^{222}Rn and stable isotopes. Hydrology and Earth System Sciences, 22, 5579–5598.

Meinikmann, K., Hupfer, M., & Lewandowski, J. (2015). Phosphorus in groundwater discharge–A potential source for lake eutrophication. Journal of Hydrology, 524, 214–226.

Olid, C., Rodellas, V., Rocher-Ros, G., Garcia-Orellana, J., Diego-Feliu, M., Alorda-Kleinglass, A., Bastviken, D., & Karlsson, J. (2022). Groundwater discharge as a driver of methane emissions from Arctic lakes. Nature communications, 13(1), 3667.

Qin, B., Zhou, J., Elser, J. J., Gardner, W. S., Deng, J., & Brookes, J. D. (2020). Water depth underpins the relative roles and fates of nitrogen and phosphorus in lakes. Environmental Science & Technology, 54(6), 3191–3198.

Rosenberry, D.O., Lewandowski, J., Meinikmann, K., & Nützmann, G. (2015). Groundwate -the disregarded component in lake water and nutrient budgets. Part 1: effects of groundwater on hydrology. Hydrological Processes, 29, 2895–2921.

Schmidt, A., Gibson, J.J., Santos, I.R., Schubert, M., Tattrie, K., & Weiss, H. (2010). The contribution of groundwater discharge to the overall water budget of two typical Boreal lakes in Alberta/Canada estimated from a radon mass balance. Hydrology and Earth System Sciences, 14(1), 79–89.

Shi, X., Luo, X., Jiao, J. J., & Zuo, J. (2022). Dominance of evaporation on lacustrine groundwater discharge to regulate lake nutrient state and algal blooms. Water Research, 219, 118620.

Stets, E. G., Winter, T. C., Rosenberry, D. O., & Striegl, R. G. (2010). Quantification of surface water and groundwater flows to open-and closed-basin lakes in a headwaters watershed using a descriptive oxygen stable isotope model. Water Resources Research, 46(3).

Sun, X., Du, Y., Wu, J., Xu, J., Tian, H., Deng, Y., & Wang, Y. (2024). Two-decadal variability of lacustrine groundwater discharge: Coupled controls from weather and hydrologic changes. Water Resources Research, 60(10), e2024WR037173.

Sun, X., Du, Y., Xu, J., Tian, H., Deng, Y., Gan, Y., & Wang, Y. (2025). Control of groundwater-lake interaction zone structure on spatial variability of lacustrine groundwater discharge in oxbow lake. Water Resources Research, 61(1), e2024WR039334.

Tao, Y., Deng, Y., Du, Y., Xu, Y., Leng, Z., Ma, T., & Wang, Y. (2020). Sources and enrichment of

https://doi.org/10.5194/egusphere-2025-5433
Preprint. Discussion started: 18 November 2025

phosphorus in groundwater of the Central Yangtze River Basin. Science of the Total Environment, 737, 139837.

Tecklenburg, C., & Blume, T. (2017). Identifying, characterizing and predicting spatial patterns of lacustrine groundwater discharge. Hydrology and Earth System Sciences, 21, 5043–5063.

Tian, H., Du, Y., Deng, Y., Sun, X., Zhu, S., Xu, J., & Wang, Y. (2025). Seasonal Dynamics of Methane Fluxes from Groundwater to Lakes: Hydrological and Biogeochemical Controls. Water Research, 268, 122679.

Walvoord, M. A., & Striegl, R. G. (2007). Increased groundwater to stream discharge from permafrost thawing in the Yukon River basin: Potential impacts on lateral export of carbon and nitrogen. Geophysical Research Letters, 34(12).

Wang, Q., Li, H., Zhang, Y., Wang, X., Zhang, C., Xiao, K., & Qu, W. (2019). Evaluations of submarine groundwater discharge and associated heavy metal fluxes in Bohai Bay, China. Science of the total environment, 695, 133873.

Xiong, L., Aldahan, A., Qian, R., Yi, P., Chen, X., Li, K., & He, P. (2023). Spatio-temporal patterns and quantification of lake–groundwater interaction determined in a large water transfer lake. Hydrological Processes, 37(4), e14867.

Xu, R., Du, Y., Wang, Z., Sun, X., Yang, L., Liu, J., & Gan, Y. (2025). Contrasting lacustrine groundwater discharge in two small perennial lakes around dried-up Chahannaoer Lake, Northern China. Journal of Hydrology: Regional Studies, 58, 102280.

Xue, P., Wen, Z., Zhao, D., Jakada, H., Liang, X. (2021). Determination of hydraulic conductivity and its spatial variability in the Jianghan Plain using a multi-format, multi-method approach. Journal of Hydrology, 594, 125917.

Zedler, J.B., & Kercher, S. (2005). Wetland Resources: Status, Trends, Ecosystems Services, and Restorability. Annual Review of Environment and Resources, 30, 39–74.

Zheng, J., Chen, K., Wu, J., & Wu, J. (2025). Lacustrine groundwater discharge as an important hidden source of nutrients to a large eutrophic lake: Implications for eutrophication management. Science of The Total Environment, 960, 178313.